Published online 11 June 2018

Nucleic Acids Research, 2018, Vol. 46, No. 17 ***9081–9093***
doi: 10.1093/nar/gky495

Dimerization confers increased stability to nucleases in 5′ halves from glycine and glutamic acid tRNAs

Juan Pablo Tosar[1,2,*,†], Fabiana Gámbaro[1,2,†], Leonardo Darré[1,3], Sergio Pantano[3], Eric Westhof[4] and Alfonso Cayota[1,5,*]

[1]Functional Genomics Unit, Institut Pasteur de Montevideo, Montevideo 11400, Uruguay, [2]Nuclear Research Center, Faculty of Science, Universidad de la República, Montevideo 11400, Uruguay, [3]Group of Biomolecular Simulations, Institut Pasteur de Montevideo. Montevideo 11400, Uruguay, [4]Architecture et Réactivité de l'ARN, Université de Strasbourg, Institut de biologie moléculaire et cellulaire du CNRS, 15 rue René Descartes, 67084 Strasbourg, France and [5]Department of Medicine, Faculty of Medicine, Universidad de la República, Montevideo 11600, Uruguay

Received February 06, 2018; Revised May 16, 2018; Editorial Decision May 18, 2018; Accepted May 22, 2018

ABSTRACT

We have previously shown that 5′ halves from tRNA$^{Gly}_{GCC}$ and tRNA$^{Glu}_{CUC}$ are the most enriched small RNAs in the extracellular space of human cell lines, and especially in the non-vesicular fraction. Extracellular RNAs are believed to require protection by either encapsulation in vesicles or ribonucleoprotein complex formation. However, deproteinization of non-vesicular tRNA halves does not affect their retention in size-exclusion chromatography. Thus, we considered alternative explanations for their extracellular stability. In-silico analysis of the sequence of these tRNA-derived fragments showed that tRNA^{Gly} 5′ halves can form homodimers or heterodimers with tRNA^{Glu} 5′ halves. This capacity is virtually unique to glycine tRNAs. By analyzing synthetic oligonucleotides by size exclusion chromatography, we provide evidence that dimerization is possible *in vitro*. tRNA halves with single point substitutions preventing dimerization are degraded faster both in controlled nuclease digestion assays and after transfection in cells, showing that dimerization can stabilize tRNA halves against the action of cellular nucleases. Finally, we give evidence supporting dimerization of endogenous tRNA$^{Gly}_{GCC}$ 5′ halves inside cells. Considering recent reports have shown that 5′ tRNA halves from Ala and Cys can form tetramers, our results highlight RNA intermolecular structures as a new layer of complexity in the biology of tRNA-derived fragments.

INTRODUCTION

Since the discoveries that small regulatory RNAs can be secreted, transported in the extracellular space, and still regulate gene expression in recipient mammalian cells (1), the interest in the study of extracellular or circulating RNAs has grown evenly. This interest is mostly based on the diagnostic potential of circulating small RNAs (2) and on their biological role in RNA-mediated intercellular communication between distant cells (3).

The RNA backbone is susceptible to hydrolysis and enzymatic cleavages, especially in the extracellular space characterized by a rather high RNase activity (4). Thus, extracellular RNAs need protection from degradation in order to be transported between non-adjacent cells, and this is typically achieved by either encapsulation in lipid membrane vesicles (i.e. extracellular vesicles, EVs) (1), lipoprotein particles (5), or by their association with RNA-binding proteins (6,7). These different mechanisms confer not only alternative possibilities for RNA secretion and extracellular dynamics, but might also impact directly in the signaling potential of extracellular RNAs.

For these reasons, we have previously used high-throughput sequencing to study the small RNA content present in different types of EVs (exosomes and microvesicles) or in the extracellular non-vesicular fraction obtained from malignant and non-malignant breast cell lines (8). Interestingly, we found that the most abundant extracellular small RNAs (as confirmed by ligation-independent RT-digital PCR) were tRNA-derived fragments. Moreover, these extracellular small RNAs were mostly not associated with EVs, as their highest relative abundances were observed in the 100 000 × g supernatants of the cell-conditioned medium. In that fraction, 90% of the tRNA-derived reads corresponded to 5′ halves from tRNA$^{Gly}_{GCC}$ and tRNA$^{Glu}_{CUC}$.

*To whom correspondence should be addressed. Tel: +598 25220910; Fax: +598 25224185; Email: cayota@pasteur.edu.uy
Correspondence may also be addressed to Juan Pablo Tosar. Tel: +598 25220910; Fax: +598 25224185; Email: jptosar@cin.edu.uy
†The authors wish it to be known that, in their opinion, the first two authors should be regarded as Joint First Authors.

Although initially regarded as non-specific degradation products, tRNA-derived fragments are ubiquitous and highly abundant. This large population of small RNAs has been shown to elicit gene regulation functions acting at multiple levels in different organisms. In mammals, the RNaseA family member Angiogenin was shown to be enzyme responsible for stress-induced tRNA cleavage in the anticodon loop (9,10), and the resulting tRNA halves were shown to inhibit translation initiation by interfering with 5′ cap recognition (11). They also protect cells from apoptosis by binding to cytochrome *c* (12), induce a neuroprotective stress granule-dependent response (13), or regulate cell proliferation (14) and mRNA turnover (15). Short tRNA-derived sequences can regulate ribosome biogenesis by affecting the structure and translation efficiency of ribosomal protein mRNAs in an Argonaute-independent manner (16). A similar mechanism was previously reported for the regulation of aspartyl-tRNA synthetase mRNA processing by a misfolded $tRNA^{Asp}$ isodecoder (17), suggesting that tRNAs and their fragments also regulate mRNA structure and stability (18). Recently, 5′ halves from $tRNA^{Gly}_{GCC}$ were described in seminal plasma and shown to be transferred to mouse oocytes during fertilization (19). In the embryos, these tRNA halves were capable of silencing genes controlled by retroactive transposable elements, thus playing a role in epigenetic inheritance. Strikingly, the same tRNA halves are the ones enriched in the non-EV fraction of cancer-cell conditioned medium (8). With a least one function already known for these specific tRNA halves, their enrichment in the non-EV fraction of cell-conditioned medium implies the existence of an unknown mechanism conferring stability against nuclease degradation.

In this work, we aim to understand how certain tRNA halves achieve unusual stability, enabling them to exist as functionally relevant extracellular (and also intracellular) entities. The first option in extracellular RNA biology is to think in extracellular vesicles as carriers that protect encapsulated RNAs from degradation by extracellular nucleases. However, this does not explain the presence of tRNA halves in the 100 000 × g supernatants of the conditioned medium of different cell lines (8) or in vesicle-depleted serum (20). Formation of ribonucleoprotein complexes can also explain extracellular RNA stability, as shown for miRNAs (7,21). The possibility that RNAs themselves form particular 3D structures rendering them more resistant to degradation is less studied, though there are very elegant examples in viruses (22). In this regard, terminal oligoguanine motif-containing tRNA halves were recently shown to form stable G quadruplex-mediated intermolecular tetramers (23). Here we show that 5′ halves from $tRNA^{Gly}_{GCC}$ and $tRNA^{Glu}_{CUC}$ can homo- or heterodimerize in solution, widening the structure/function dependency of this small RNA family.

MATERIALS AND METHODS

Reagents

Ribonuclease A was obtained from Sigma, and RNase T1 (100 000 U/ml) was from Roche. Exonuclease T and Murine RNase inhibitor (40 U/μl) were from New England Biolabs. *N*-Methylmesoporphyrin IX (NMM) was obtained from Frontier Scientific. Sterile Phosphate buffered saline, PBS (purchased as 10X DPBS), DMEM, trypsin–EDTA solution, fetal bovine serum and nuclease-free distilled water were obtained from Gibco.

Cell culture

MCF-7 cells were purchased from ATCC and used at low passage (<10). Cells were routinely incubated in a humidified chamber at 37°C with 5% CO_2 without antibiotics. The cells were cultured in DMEM + 10% FBS until the desired cell number was obtained. After media removal and rinsing with phosphate buffered saline (PBS), cells were changed to defined media: Mammary Epithelial Growth Medium (MEGM, Lonza Clonetics) without the addition of the bovine pituitary extract included in the kit. After an adaptation period of 48 h, the media was completely removed, cells were rinsed with PBS and new defined media was added. After further incubation for 48 h, the cell conditioned medium was collected and centrifuged at 800 × g before storing the supernatants at –20°C.

Purification of extracellular tRNA halves and SEC analysis

Except for the results shown in Figure 1A and B, the cell conditioned medium was always centrifuged at 2000 × g (30 min, 4°C) and then at 100 000 × g (2.5 h, 4°C) in order to obtain the extracellular EV-depleted (non-EV) fraction, as previously reported and characterized (8). The supernatants were concentrated by ultrafiltration (Vivaspin 20, MWCO 5 kDa, Sartorious Stedim Biotech.) by successive dilutions with PBS to remove phenol red and small molecules. Concentrated non-EV fractions (500 μl) were injected in a Superdex S75 10/300 column (Amersham) and size exlusion chromatography (SEC) was performed at 0.5 ml/min in 0.22 μm-filtered PBS with an Äkta Pure (GE healthcare) FPLC system. The same protocol was used for the analysis of synthetic RNAs. All samples were centrifuged at 16 000 × g for 10 min at 4°C before injection in the columns.

Controlled ribonuclease digestion assays

A 10μl mixture containing 100 pmol of the desired RNAs in 1× PBS was heated at 95°C for 1 min and cooled at room temperature for 30 min in order to perform unfolding/refolding of the RNAs. For RNase T1 digestion assays, 1 μl of different enzyme dilutions (in PBS, spanning 0.01–10 enzymatic units) were added, and digestion was performed at 20°C for 30 min. For exonuclease T treatment, 10 μl of different enzyme dilutions in 1× NEB Buffer 4 were added to the refolded RNAs, and the reactions were carried out for 2 h at 20°C. A 4 μl aliquot was mixed with 2× denaturing gel loading dye (Thermo Scientific) and ran in a 20% (Rnase T1) or 15% (Exonuclease T) polyacrylamide gel containing 7 M urea in 90 mM Tris-borate (TB) buffer, pH 8.3. Gels were run at 100 V for 2–3 h, and stained with 1× SYBR gold (Thermo Scientific).

RNA extraction and Stem-loop RT quantitative PCR

RNA purification was performed with Trizol LS (Invitrogen, Life Technologies) according to manufacturer's in-

structions. RNA was quantified using a Qubit 2.0 fluorometer (Life Technologies) and a Qubit RNA high sensitivity kit, according to manufacturer's instructions. Spectrophotometric quantification of extracellular RNAs was considered not reliable due to traces of phenol absorbing at 270 nm. Stem-loop RT-qPCR was performed directly in the conditioned medium (no RNA purification) or in purified RNA extracted from cells. The detailed protocol and primers used in this study are presented in the supplementary materials section.

Small RNA sequencing

RNA was purified from fractions corresponding to the 'H' (Ve = 10.2 ml) or 'L' peak (Ve = 11.5 ml) obtained after SEC purification of the MCF-7 cell conditioned medium following EV depletion. The 'H' peaks from samples treated with 40 U murine RNase inhibitor immediately upon conditioned medium collection were also analyzed. The obtained RNA was diluted in 8 μl of ultra-pure RNase-free water, and 7 μl were used as input for NGS library preparation using the NEBNext Small RNA Library Prep Set for Illumina (New England Biolabs) according to the manufacturer's instructions. Sequencing was performed in a MiSeq benchtop sequencer for 200 cycles, though small RNAs analyzed in this study were all in the 15–100 nt range. The analysis was performed as previously described (8) and stated in the supplementary materials section.

Fluorescence microscopy

MCF-7 cells (1×10^4) were seeded onto 96-well plates and 24 h later were washed with PBS and transfected with 100 nM biotinylated RNAs (WT, 9GG/AA, 25U/C and SCR) using Lipofectamine 2000 (Invitrogen) following manufacturer's recommendations. Briefly, 0.5 μl of RNA (100 μM) was mixed with 2 μl of Lipofectamine 2000, and the RNA was diluted to 100 nM in MEGM medium. After 30 min incubation with the lipid/RNA mixture, cells were rinsed three times with PBS to remove non-transfected RNA. This was defined as our zero time point ($t = 0$). After the desired experiment duration, cells were fixed using 4% paraformaldehyde for 15 min at RT and permeabilized with PBS plus 0.3% Tween-20 for 3 min. Then, cells were incubated with blocking buffer (5% BSA in PBS) for 1 h at 37°C. The cells were washed three times with PBS and incubated with streptavidin–APC diluted 1:500 in blocking buffer containing DAPI (Santa Cruz Biotechnology) for 30 min at room temperature in dark. After washing with PBS, coverslips were mounted using Prolong Gold Antifade Reagent (ThermoFisher Scientific). Cells were photographed with a Zeiss confocal microscope (Axio Observer Z1, LSM 800) using a 63× oil immersion objective and analyzed using Fiji-ImageJ software. Acquisition parameters were the same for non-transfected cells (negative control) and transfection with the four biotinylated RNAs.

Synthetic RNA oligonucleotides

Synthetic oligonucleotides were purchased from Integrated DNA Technologies (USA). The sequences of the RNAs (all bases as 2′-OH) used in this study are the following (5′–3′, mismatches underlined):

- $tRNA^{Glu}_{CUC}$ 5′ halves: UCCCUGGUGGUCUAGUGGUUAGGAUUCGGCG
- $tRNA^{Gly}_{GCC}$ 5′ halves (WT): GCAUUGGUGGUUCAGUGGUAGAAUUCUCGC
- $tRNA^{Gly}_{GCC}$ 5′ halves (9GG/AA): GCAUUGGU**AA**UUCAGUGGUAGAAUUCUCGC
- $tRNA^{Gly}_{GCC}$ 5′ halves (25U/C): GCAUUGGUGGUUCAGUGGUAGAAU**C**CUCGC
- $tRNA^{Gly}_{GCC}$ 5′ halves (SCR): G**U**AUA**G**GUG**U**GUC**G**GU**A**GUAG**U**AU**C**CUCGC

Biotinylated versions of WT, 9GG/AA, 25U/C and SCR included a 5′ biotin group. The WT sequence was also purchased with a DNA instead of a RNA backbone (2′-deoxy). WT and 25U/C oligonucleotides bearing a 5′ phosphate group were also included in specified assays. Sequences for Ala and Cys 5′ tRNA halves are the same used in Ivanov *et al.* (13).

RESULTS

Non-vesicular extracellular tRNA halves show increased nuclease stability

Previous work from our group has shown that 5′ tRNA halves are the most abundant small RNAs present in the conditioned medium of breast cell lines (MCF-7 and MCF-10A) grown in serum-free conditions (8). Furthermore, these tRNA-derived fragments were mostly enriched in the non-vesicular fraction. Strikingly, ∼90% of tRNA fragments in this fraction were derived from $tRNA^{Glu}_{CUC}$ and $tRNA^{Gly}_{GCC}$. This was not merely a technical bias, since a heterogeneous population of tRNA-derived fragments could be sequenced in the intracellular space.

We then asked whether cells were selectively secreting specific tRNA halves or whether these represented the most stable species in the extracellular space. The latter was supported by the observation that 5′ halves from $tRNA^{Gly}$ and $tRNA^{Glu}$ were not significantly degraded after overnight incubation at 37°C of collected (cell-free) MCF-7 cell conditioned medium (Figure 1A). There was a small increase in the Cq value of $tRNA^{Gly}_{GCC}$ 5′ halves, which could be reverted by addition of RNase inhibitor (Figure 1B), but such extent of degradation was considered negligible in both cases. The 5′ halves from $tRNA^{Glu}_{CUC}$ were also very stable. The small, non-significant decrease in their Cq value might be indicative of an extracellular biogenesis for these tRNA-derived fragments, but such a mechanism extends beyond the scope of this study.

To address whether the high stability of $tRNA^{Gly}$ and $tRNA^{Glu}$ 5′ halves was a consequence of a low extracellular RNase activity in MCF-7 cell conditioned medium, we purified the fraction containing the tRNA halves by size-exclusion chromatography (SEC). As we had previously reported (8), SEC analysis of the non-EV fraction of MCF-7 cell conditioned medium defined two peaks where OD260 > OD280, corresponding to high molecular weight ('H' peak, Ve = 10.2 ml, apparent MW ≈ 40 kDa) and low molecular weight ('L' peak, Ve = 11.5 ml, apparent MW

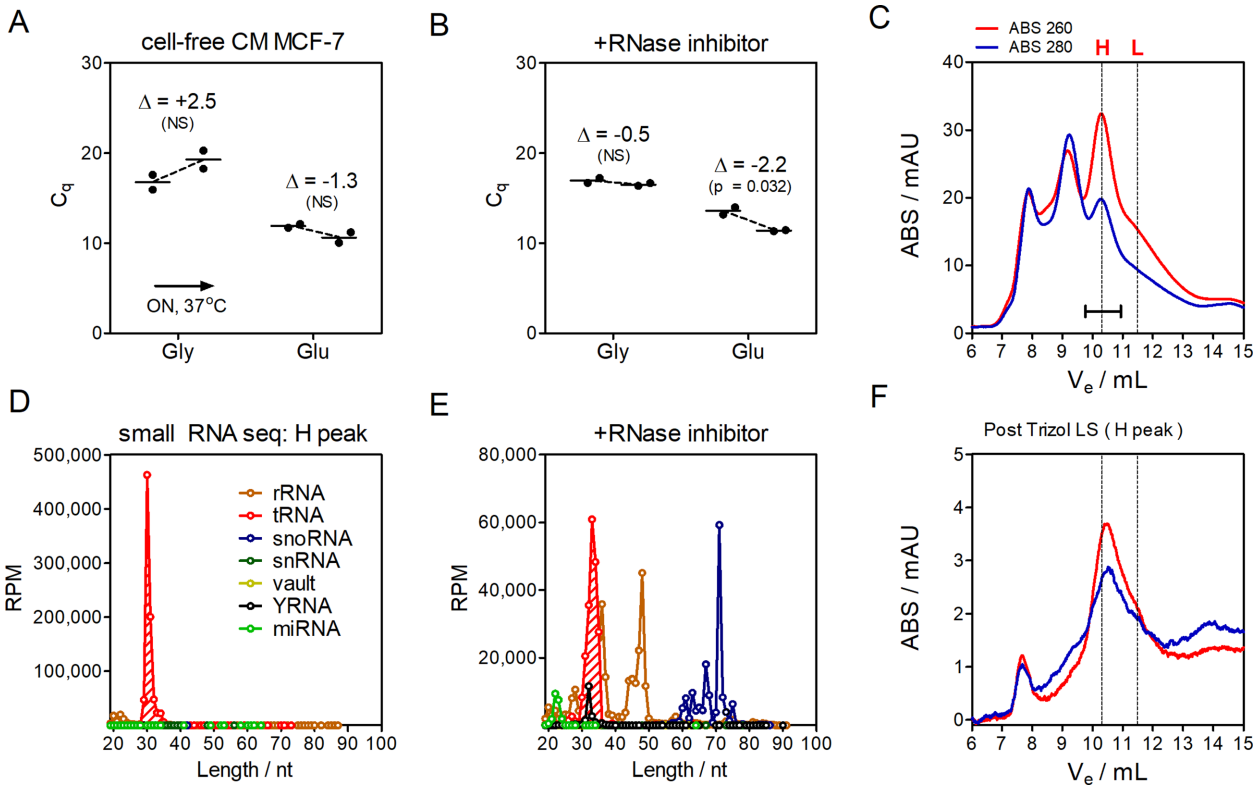

Figure 1. 5′ Halves from $tRNA^{Gly}$ and $tRNA^{Glu}$ are highly stable in the non-EV fraction from MCF-7 cell conditioned medium. (**A**) MCF-7 cells were grown under defined serum-free conditions, and cell conditioned medium was collected after 48 h. The medium was split in two aliquots, one of which was immediately stored at −20°C while the other was left at 37°C overnight (ON) and then frozen. After thawing, 600 μl aliquots were concentrated 10× by ultrafiltration (using membranes with a cut-off of 5 kDa). The tRNA halves were assayed by stem-loop RT-qPCR and their quantification cycle (Cq) values are shown. Significant or not-significant (NS) changes are indicated based on two-tailed Student t test. In a parallel experiment (**B**), 40 U of murine RNase inhibitor was added to the cell conditioned medium upon collection. (**C**) The cell conditioned medium, either with or without addition of RNase inhibitor, was centrifuged at 100 000 × g for 2.5 h and the supernatant was concentrated and injected in a Superdex S75 column. Absorbance at 260 nm and 280 nm are shown in red and blue, respectively. The peak termed 'H' was collected, RNA was extracted and the purified RNA was either used for small RNA sequencing (**D** and **E**) or reinjected in the same column (**F**). Sequencing reads were collapsed to unique sequences, classified based on their origins (mature miRNAs or fragments of rRNAs, tRNAs, snoRNA, snRNAm vault RNAs or YRNAs) and relative abundances (expressed in reads per million mapped reads, RPM) were plotted against sequence length (D and E).

≈ 20 kDa) RNase-sensitive complexes (Figure 1C). Small RNA sequencing of both peaks showed that 89.5% (H) and 82.2% (L) of mapped reads were derived from tRNAs (Figure 1D). Of these, 88.2% (in the H peak) corresponded to 5′ fragments of 28–33 nt from $tRNA^{Gly}_{GCC}$ and $tRNA^{Glu}_{CUC}$ (Supplementary Table S1). Hence, confirming our previous finding regarding the total (before SEC) non-EV extracellular fraction (8). The amplification of these tRNA halves in the 'H' and 'L' peaks was confirmed by stem-loop RT-qPCR (SL-RT-qPCR), which is independent of RNA 3′-end modifications and does not amplify intact precursors (i.e. full-length tRNAs), as explained in the Supplementary Methods section. However, when adding RNase inhibitor to the medium, a plethora of small RNAs derived from varied ncRNAs was evident, with tRNA-derived fragments representing only 30% of mapped reads (Figure 1E, note the decrease in RPM values). In particular, fragments of 28S rRNA (starting at position 1 in sequences of 36 nt, and at position 4439 in sequences defining the peak at 48 nt) and complete small nucleolar RNAs (with the C/D box U49A snoRNA being the most abundant) were almost as frequent as tRNA halves under these experimental conditions. Given that all these species are not detected in the absence of RNAse inhibitor, we conclude that tRNA halves are more stable than other RNAs of similar lengths in the extracellular compartment.

We could envision two mechanisms that would explain the high extracellular stability observed for the aforementioned tRNA halves: (a) selective binding to specific proteins to form extracellular ribonucleoprotein (RNP) complexes, or (b) adoption of particular three-dimensional structures less prone to RNase-mediated degradation. Because the elution volume of the 'L' peak (Figure 1C) is very close to that of synthetic 30 nt oligonucleotides (see below), only the 'H' peak could correspond to a RNP complex containing the tRNA halves under study. To our surprise, purification of the RNA from this peak by Trizol LS and reinjection of the purified (i.e. deproteinized) RNA did not shift its elution volume (Figure 1E). From this we concluded that tRNA halves present in the non-EV fraction do not elute as RNP complexes.

In-silico analysis predicts that 5′ halves from tRNA^{Gly} and tRNA^{Glu} form homo- and heterodimers

Although we cannot rule out the existence of low affinity RNP complexes that dissociate before or during SEC, the previous results encouraged us to consider alternative explanations to the remarkable stability of extracellular non-vesicular tRNA halves. In the absence of protective protein partners, we envisioned RNAs could gain stability against degradation by folding into specific structures governed by intra- or intermolecular RNA-RNA interactions. The former case was shown for ncRNAs derived from flavivirus, where the adoption of specific folds protects the RNAs from the action of intracellular nucleases (22). To study this, we first performed *in silico* predictions of the most stable secondary structures these tRNA halves could adopt.

Analysis of 5′ halves from tRNA$^{Gly}_{GCC}$ and tRNA$^{Glu}_{CUC}$ with *mFold* (24) predicted stable stem-loop structures comprising, respectively, nucleotides 2–17 and 2–18 with the same UGGU tetraloop in both cases (Figure 2A). The rest of the molecule did not show any predictable stable secondary structures. However, the unstructured segment showed near perfect self-complementarity, with an uninterrupted 8 nucleotide-long stretch of Watson and Crick or G:U pairing in the tRNA$^{Gly}_{GCC}$ 5′ halves (Figure 2B), as predicted by the *bifold* algorithm form the RNAstructure web server (http://rna.urmc.rochester.edu/RNAstructureWeb/). This suggest that tRNA halves from certain glycine acceptors have a sequence that is amenable to homodimerization, while heterodimerization is attainable in the case of Gly/Glu tRNA halves (Figure 2, C). An inspection of the Modomics database (http://modomics.genesilico.pl/) of mature tRNA post-transcriptional modifications did not show reported modified bases in the tRNA precursors that could interfere with base pairing interactions in the dimerization interface (Figure 2C).

To provide further insight into the ability of these 5′ tRNA halves to form dimers, unrestrained *ab initio* three-dimensional folding simulations using *simRNA* (25) were performed as described in Supplementary Methods. Such calculations provide 3D structural models that can be further used to explore dimer dynamics and interactions with other macromolecules or ligands. The main folded state predicted by this method corresponded to *bifold* predictions for tRNA^{Gly} homodimers (Figure 2D and Supplementary Figure S1). The main folded state for Gly/Glu heterodimers also resembled *bifold* predictions, with equivalent population as for Gly/Gly homodimers (Figure 2E). Noteworthy, the ability of these structures to hide their 3′ ends could render them less prone to degradation by cellular 3′–5′ exonucleases. In agreement with *bifold*, tRNA^{Glu} homodimers were less favored by *simRNA*, with a 2-fold reduction in the population associated to the main folded state (Supplementary Figure S1).

To address whether tRNA 5′ halves dimerization ability is a consequence of the high G/C/U content of tRNAs instead of a specific feature of tRNA$^{Gly}_{GCC}$ and tRNA$^{Glu}_{CUC}$, *bifold* calculations were applied to all predicted human tRNA genes from the genomic tRNA database (GtRNAdb, comprising 610 predicted tRNA genes in the human genome version hg19), to assess the capacity of their 5′ halves to form homodimers. For ranking this in a genome-wide scale, mature tRNA sequences were truncated to thirty nucleotides from their 5′ end and then the percentage of bases forming intra- or inter-molecular base pairing interactions was computed. From the starting 346 non-redundant 30 nt sequences, only 9 showed a percentage of dsRNA content ≥80%, and three of these sequences were 5′ fragments from different tRNA$^{Gly}_{GCC}$ sequences (Supplementary Figure S2). This means that 5′ tRNA halves are not, in general, capable of forming the kind of homodimers that we predicted for tRNA$^{Gly}_{GCC}$.

To rule out a possible bias in restricting only to 30 nt 5′ tRNA fragments, we studied the most abundant tRNA-derived sequences present in the intracellular compartment of MCF-7 cells, irrespectively of their length and start position. In this case, only tRNA^{Gly}-derived sequences of 30 nucleotides reached an 80% of dsRNA bases, while tRNAs accepting amino acids other than glycine scored much lower (Figure 3). Moreover, the tRNA^{Gly}-derived sequences that maximized their homodimer forming potential corresponded to those being more abundant in the extracellular (but not the intracellular) space. Thus, the bias towards 5′ halves from tRNA^{Gly} in the extracellular milieu could be a consequence of their specific capacity to form homodimers, what could render them less sensitive to single-stranded endonucleases (e.g. RNaseA family members).

5′ halves from tRNA^{Gly} dimerize spontaneously *in vitro*

To verify the *in-silico* predictions, we first determined the expected elution volume for labelled single-stranded and double-stranded short (<30 nt) oligonucleotides by SEC, and defined dimer (D) and monomer (M) elution volumes by analyzing the shift in the 260 and 495 nm (6-FAM) absorbance (Supplementary Figure S3).

Mimics of tRNA$^{Gly}_{GCC}$ 5′ halves (of either 30 or 31 nucleotides) defined a bimodal profile with maximums close to the D and M peaks (Figure 4A). As expected for monomer-dimer equilibrium, the D/M ratio increased as a function of the concentration of injected RNA (Figure 4B). This behavior was not dependent on the presence or absence of a 5′ phosphate group (Supplementary Figure S4A). Importantly, the absorbance of the D peak grew linearly with the square of the absorbance of the M peak (Supplementary Figure S4B), which is characteristic and expected in a monomer-dimer equilibrium (Supplementary Figure S4D). With the empirically calculated molar extinction coefficient of the RNA, we determined a dissociation constant of approx. 3μM for these dimers in PBS. Of note, the RNAs aggregated under conditions typically used for native gel electrophoresis, as evidenced by SEC analysis in 90 mM Tris-borate buffer pH 8.3 (data not shown). Thus, SEC was considered as the most suitable technique to study these tRNA-derived fragments under pH and osmolarity conditions representative of the extracellular space (PBS).

To validate our predictions, we designed a mutant in the dimerization interface by substituting a uracil for a cytosine (25U/C mutant). As expected, the behavior of this mutant was exclusively monomeric (Figure 4A). However, this mutant was designed in order to keep complementarity with tRNA$^{Glu}_{CUC}$ 5′ halves, which do not form homod-

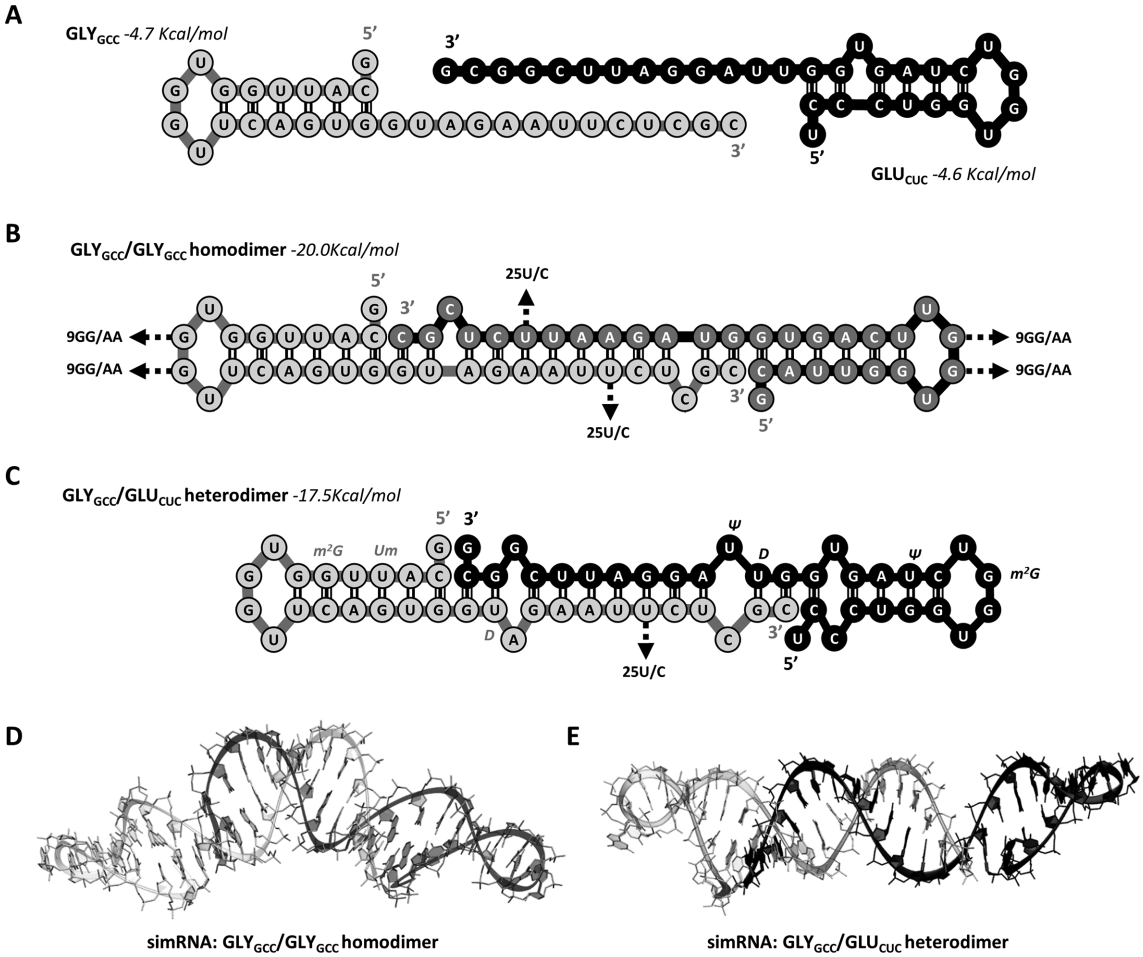

Figure 2. Predicted secondary structures and putative dimers of the most abundant 5′ halves from tRNA^{Gly} and tRNA^{Glu} found in the conditioned medium of MCF-7 cells. (**A**) Most stable secondary structures of the monomers, as predicted by *mFold*. (**B**) Homodimers of tRNA$^{Gly}_{GCC}$ 5′ halves, as predicted by *Bifold*. Arrows show the substituted bases in the mutants (25U/C and 9GG/AA) used in this study. (**C**) Heterodimers of tRNA$^{Gly}_{GCC}$ and tRNA$^{Glu}_{CUC}$ 5′ halves. Modified bases in the tRNA precursors (according to the *Modomics* database) are superimposed. The arrow shows the 25U/C mutant, which cannot homodimerize but can still form heterodimers with 5′ halves from tRNA$^{Glu}_{CUC}$. (D, E) Representative structures of the main folded state of Gly/Gly homodimers (**D**) and Gly/Glu heterodimers (**E**) as predicted by *ab initio* bi-molecular simulations using *simRNA*.

imers. Consequently, an equimolar mixture of tRNA$^{Glu}_{CUC}$ 5′ halves and the 25U/C mutant still retained absorbance in the dimer elution volume (Supplementary Figure S5). Finally, a second mutant (9GG/AA) where both guanines are swapped for adenines in the UGGU tetraloop (which does not participate in putative dsRNA interactions) showed a dimerization capacity that was comparable to the wild-type sequence (Figure 4A), strongly supporting *in-silico* structural predictions (Figure 2 and Supplementary Figure S1).

UV-melting experiments defined a melting temperature of 46.4°C for Gly/Gly homodimers, which was consistent with the melting temperature (47.8°C) measured by differential scanning calorimetry (Supplementary Figure S6). Both assays were performed at micromolar RNA concentrations to ensure the majority of molecules were initially present as dimers.

Dimerization of 5′halves from tRNA^{Gly} is dependent on the RNA 2′-OH hydroxyl group

It was reported that tRNA halves of Ala and Cys are capable of forming G-quadruplex-containing structures that promote stress granule formation and protect motor neurons. Interestingly, synthetic oligonucleotides with DNA instead of RNA backbone (but with uracil instead of thymine) were shown to retain these structural and functional properties (13). We tested whether mimics of 5′ halves from tRNA$^{Gly}_{GCC}$ were able to dimerize when they bear a DNA (2′-deoxy) backbone but negligible absorbance at the dimer peak was obtained in that case (Supplementary Figure S7). This observation suggested the involvement of the ribose hydroxyl group in specific local RNA folds besides the expected base pairs and the additional stabilization of the dimers.

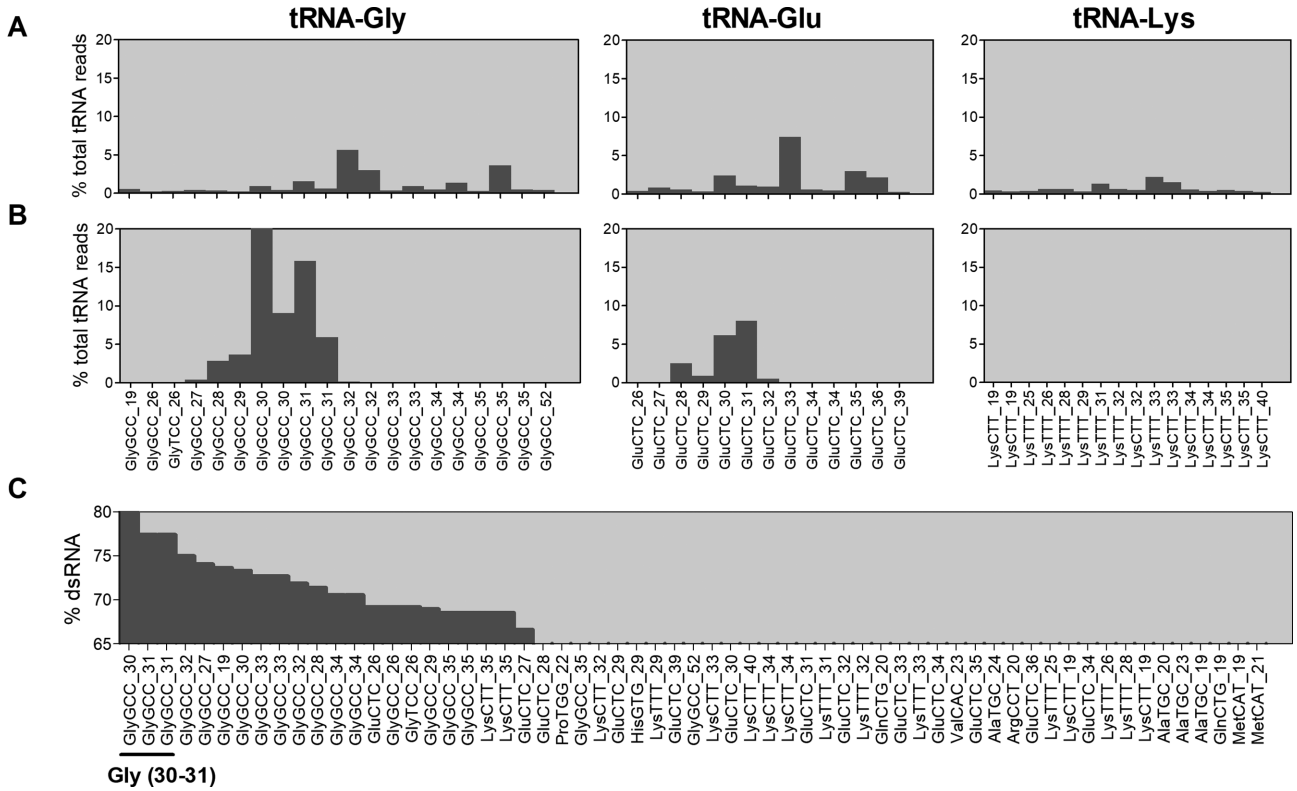

Figure 3. The tRNA fragments enriched in the extracellular space (non-EV fraction) are those with a higher dimerization potential. Histograms represent the percentage of total tRNA-derived reads in the intracellular (**A**) or the extracellular non-vesicular fraction (**B**) of MCF-7 cells. For all tRNA-derived sequences detected in the intracellular fraction, a prediction of their dimerization potential was performed by forcing the formation of homodimers using *bifold* (**C**) and ranking each unique sequence by the percentage of intra- or inter-molecular paired bases (%dsRNA). Unique sequences were labelled based on the tRNA they were presumably derived from and based on their size (i.e., tRNA_size). Sequences with the same size but corresponding to different tRNA isodecoders were treated separately but given the same name.

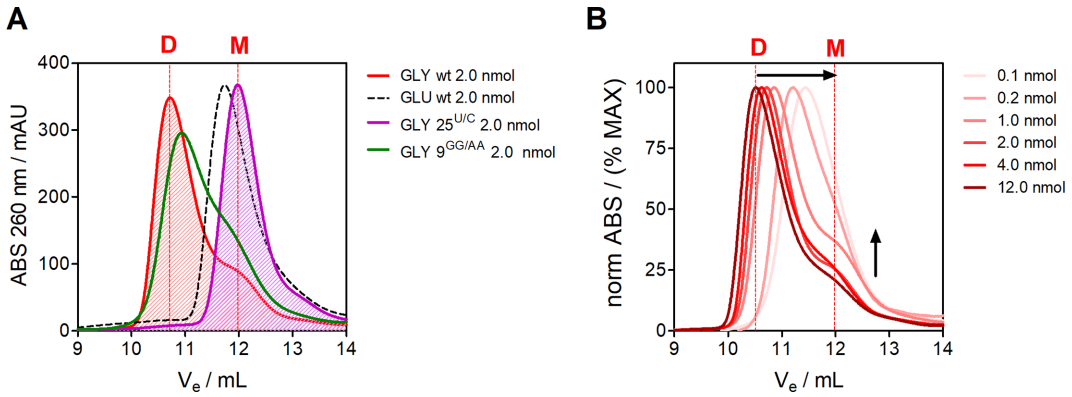

Figure 4. Synthetic unmodified $tRNA^{Gly}_{GCC}$ 5′ halves form homodimers *in vitro*. (**A**) Chromatograms show OD260 curves for sequences corresponding to wild-type $tRNA^{Gly}_{GCC}$ 5′ halves (red) and the 25U/C and 9GG/AA mutants (violet and green, respectively). A RNA oligonucleotide bearing the sequence of $tRNA^{Glu}_{CUC}$ 5′ halves is shown in black (dashed line). (**B**) Normalized chromatograms (maximum absorbance = 100%) of successive injections of synthetic $tRNA^{Gly}_{GCC}$ 5′ halves, spanning 0.1–12.0 nmol (light red – dark red). Arrows show how dilution provokes an increase of the monomer (M)/dimer (D) ratio, with the maximum absorbance shifting to higher elution volumes as a consequence of decreasing absorbance at the dimer peak.

5′-Halves from $tRNA^{Ala}$ and $tRNA^{Cys}$ form tetramers but not 5′ halves of $tRNA^{Gly}$

A recent report has provided further insights on the G-quadruplex containing structures formed by $tRNA^{Ala}$ and $tRNA^{Cys}$ 5′-halves (23). It was shown that the terminal oligoguanine motif present in these sequences enabled the formation of denaturation-resistant intermolecular tetramers stabilized by five consecutive G tetrads. We thought to use SEC to reproduce these findings, which were mostly based on electrophoretic mobility. DNA backbone (2′-deoxy)-containing oligonucleotides corresponding to 5′ halves of $tRNA^{Ala}$ and $tRNA^{Cys}$ showed again two peaks, but no absorbance in the dimer region. In contrast, elution vol-

umes were consistent with monomer-tetramer equilibrium in this case (Supplementary Figure S8A). Moreover, incubation with the G-quadruplex labeling compound N-methylmesoporphyrin IX (NMM) showed the label exclusively associated with the oligomer peak, thus confirming the main findings of Lyons *et al.* (23). Oligonucleotides mimicking 5′ halves of $tRNA^{Ala}$ and $tRNA^{Cys}$ were able to shift the absorbance maximum of NMM in solution from 378 (free) to 499 (bound) nm, while 5′ halves of $tRNA^{Gly}$ did not (Supplementary Figure S8B), indicating the lack of tetramerization of the latter.

Dimers of $tRNA^{Gly}$ 5′ halves are more resistant to RNase T1 digestion

To address whether dimer formation contributes to the stability of tRNA halves, we compared the *in vitro* sensitivity to RNase T1 digestion of synthetic 5′ $tRNA^{Gly}_{GCC}$ halves, the 25U/C and the 9GG/AA mutants. Since RNase T1 performs endonucleolytic cleavage adjacent to guanine bases in single-stranded RNAs, we hypothesized that the 9GG/AA mutants should be the most resistant, since these oligonucleotides are able to form dimers that do not carry single-stranded guanines. In contrast, we expected the 25U/C mutants to be degraded the fastest, as their inability to form dimers exposes a higher number of single-stranded guanines. However, since the putative dimers are present in dynamic equilibrium with their respective monomers, all RNAs should be degraded in prolonged digestions. Thus, we first optimized reaction conditions in order to obtain only partial, controlled degradation of the oligonucleotides.

The appearance of a transient degradation product (termed 'I', showing an elution volume of ≈ 13 ml) was evident for both the 25U/C and 9GG/AA mutants, but non-detectable in the wild-type $tRNA^{Gly}$ 5′ halves (Figure 5A). When increasing the amount of RNase T1 10-fold, this intermediate was lost, and all absorbance at 260 nm shifted to elution volumes ≥14.0 ml, corresponding to fully degraded products. Considering this intermediate could correspond to the stem-loop structure predicted in position 2–17 of $tRNA^{Gly}$ 5′ halves, their lack of detection in the wild-type sequences is consistent with the UGGU tetraloop being the unique RNase T1 target site in the dimers.

For controlled RNase T1 digestion experiments, we decreased the temperature to 20°C to reduce the fraction of molecules in monomeric state, and increased the amount of RNase T1 in order to assure detection of the 'I' peak in 9GG/AA mutants. Under such conditions, ∼25% of the absorbance of 9GG/AA mutants remained below an elution volume of 14.0 ml (i.e. not forming fully-degraded products). This was significantly higher ($P < 0.001$) than the number of remaining oligonucleotides after digestion of wild-type sequences in parallel experiments (Figure 5B). This supports our prediction that the UGGU tetraloop spanning positions 8–11 is the only guanine-containing single-stranded sequence in the dimers under study. In contrast, 25U/C mutants were almost entirely degraded under the same conditions, confirming our predictions.

Enzymatic digestions conditions were scaled for the analysis of digested products by denaturing gel electrophoresis, as explained in methods. At 1U RNase T1, the 25U/C mutants were completely digested, while digestion intermediates (lost at higher enzyme concentrations) were still evident in the wild-type sequence (Figure 5C). In agreement with SEC results, the 9GG/AA mutant was the most stable, with intact oligonucleotides still present at 1 U RNase T1.

Analysis of endonuclease/exonuclease digestion products supports structural models.

Besides confirming differential stabilities against RNase T1 (with 9GG/AA > WT > 25U/C), we asked whether the digestion intermediates identified in Figure 5C were consistent with our structural models and the rationale summarized in Figure 5D. If, according to our previous claim, the UGGU tetraloop is the only RNase T1 target site within the WT $tRNA^{Gly}$ dimers, this would result in a transient product of 20 or 21 nucleotides (depending on which of the two guanines is cleaved). This is evident from Figure 5C, and also appears as a major intermediate at very low (0.01 U) enzyme concentrations (Supplementary Figure S9A). This intermediate was never observed in the 9GG/AA mutant. In contrast, the band of approximately 18 nt (Figure 5C, and Supplementary Figure S9, A) possibly corresponds to the stem–loop structure of the monomer, which we previously termed 'I' by SEC (Figure 5A), and is mutually exclusive with the 20–21 nt product observed in the WT sequence.

To gain further insights, we treated RNAs with the 3′-5′ single stranded Exonuclease T. This enzyme is used to generate blunt ends in dsRNAs containing 3′ overhangs, meaning it stops when reaching the first double-stranded RNA interaction starting from the 3′ end. As a control for this activity, we tested a scrambled version of $tRNA^{Gly}$ (SCR), which does not dimerize but contains three predicted dsRNA interactions at its 3′ end. As expected, no cleavage was observed (Supplementary Figure S9B), demonstrating lack of residual endonuclease activity in the enzyme. In contrast, WT oligonucleotides were degraded to a product of approximately 17 nt (i.e. lost 13 nt from their 3′ end), which corresponds to the stem loop structure of the monomer, which is the predicted substrate of the enzyme (Supplementary Figure S9B and C). Presumably as a consequence of an internal folding in the monomer 3′ tail, only two nucleotides were cleaved in the 25U/C mutants. Although this interaction is also possible in the WT sequence, its formation competes with enzymatic digestion, as dissociation of the dimer and degradation of the monomer are in dynamic equilibrium. In any case, it should be noted that the 3′ end of the WT sequence is less exposed than in the 25U/C mutant, as 2.5 enzymatic units preserve most of the former while completely transforming the latter to a mixture of -1 and -2 nt products (Supplementary Figure S9C).

Dimerization capacity dictates the intracellular turnover of $tRNA^{Gly}$ 5′ halves

The previous results do not only provide strong support to the structures shown in Figure 2, but also demonstrate that dimerization contributes to the resistance of these tRNA halves towards single-stranded endonucleases. To study this in a more biologically-relevant scenario (which

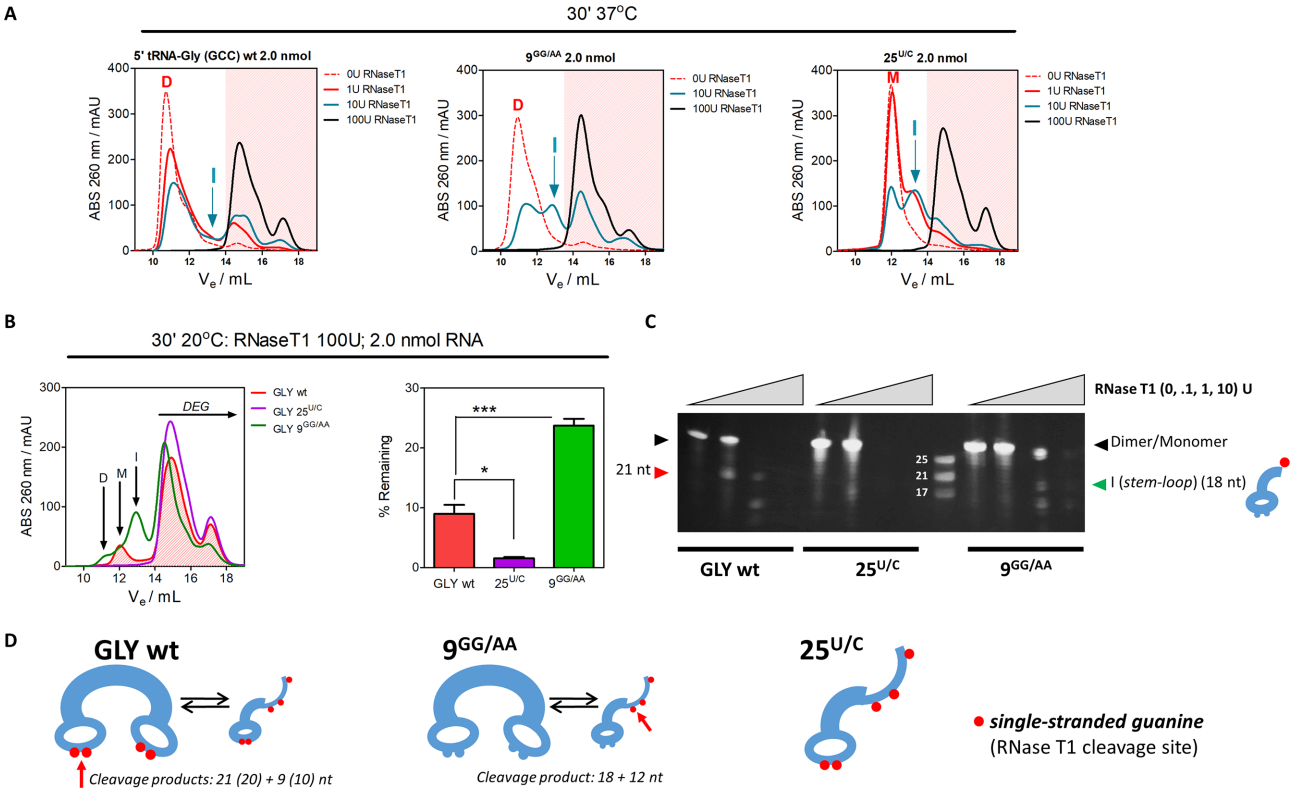

Figure 5. Controlled RNase T1 digestion of $tRNA^{Gly}_{GCC}$ 5′ halves and selected mutants show dimerization capacity correlates with resistance to endonuclease cleavage. (**A**) Increasing amounts of RNase T1 (30 min, 37°C) show transient appeareance of a partial digestion product (termed 'I') in the 25U/C and 9GG/AA mutants, and full-degradation products with elution volumes higher than 14.0 ml (shaded in red). D, M, I: dimer, monomer, and intermediate, respectively. (**B**) Controlled digestion with 100U RNase T1 at 20°C of equimolar quantities of wild-type $tRNA^{Gly}_{GCC}$ 5′ halves (red), the 25U/C mutant (violet), and the 9GG/AA mutant (green). The absorbance at elution volumes below 14.0 ml (not fully-degraded products) was quantified and expressed as the percentage of total absorbance at 260 nm. One-way ANOVA with Tukey post-hoc test was performed to address statistical significance in three replicates of each experiment (*$P < 0.05$, ***$P < 0.0001$). (**C**) Digestion of heat-denatured and room temperature refolded 100 pmol RNA oligonucleotides diluted in 1× PBS with varying amounts (0, 0.1, 1 and 10 enzymatic units) of RNAse T1 for 30 min at 20°C. Digested products were analyzed in a 20% denaturing (7 M urea) polyacrylamide gel. The mutuallyexclusive 21 and 18 nt intermediates are shown with red and green arrows, respectively. (**D**) Schematic representation of predicted RNase T1 cleavage sites in dimers and monomers of the oligonucleotides used in this study, indicating the sizes of the expected primary products after cleavage at the indicated positions. The red dots indicate the presence of single-stranded guanines.

includes a cocktail of endo and exonucleases), we transfected MCF-7 cells with 5′ biotinylated versions of wild-type 5′ halves of $tRNA^{Gly}$ (WT), the 25U/C and 9GG/AA mutants, and a scrambled (SCR) version of $tRNA^{Gly}$ 5′ halves, where different bases were shuffled in order to prevent any stable secondary structures and alter the dimerization interface. A lipofectamine-RNA (100 nM) mixture was incubated with the cells for 30 min, fresh medium was added ($t = 0$), and immunofluorescence microscopy was performed at different time points, using a Streptavidin-APC conjugate to detect and quantify transfected RNA. As evidenced by the cell area-normalized total APC fluorescence at $t = 0$, transfection efficiencies were comparable for the four tested RNAs. At 6 h post transfection, SCR and 25U/C mutants (dimerization incompetent) were decreased to basal (i.e. non-transfected) levels. In contrast, WT and 9GG/AA oligonucleotides (dimerization competent) were not degraded to any significant level (Figure 6A, B, D). Similar results were obtained by performing relative quantization of WT and SCR sequences by SL-RT-qPCR (Figure 6C). The fast turnover of dimerization incompetent RNAs was due to intracellular degradation and not a consequence of preferential secretion, as extracellular levels of SCR were also much lower than WT (Figure 6E).

$tRNA^{Gly}$ 5′ halves elute as dimers in MCF-7 cell lysates

To assess whether endogenous $tRNA^{Gly}_{GCC}$ 5′ halves exist as monomers or dimers inside a cell, we lysed MCF-7 cells under conditions which would denature proteins while preserving RNA intermolecular interactions (PBS + 0.1% SDS). Cell pellets were resuspended in cold lysis buffer, passed successively through a syringe needle and filtered by 0.22 μm. The lysates were analyzed by SEC under non-denaturing conditions (PBS) and a representative chromatogram is shown in Figure 7A. We hypothesized that the OD260 peak at Ve = 10.0 ml corresponds to full-length mature tRNAs, and confirmed this by injecting a gel-purified commercial yeast $tRNA^{Phe}$ standard (Figure 7A, inset).

Given that synthetic 5′ halves from $tRNA^{Gly}_{GCC}$ bearing a 5′ phosphate defined a dimer peak at Ve = 10.3 ml in the same column (Supplementary Figure S4), we had a narrow but still useful margin to discriminate between dimers of tRNA halves and the highly abundant full-length mature

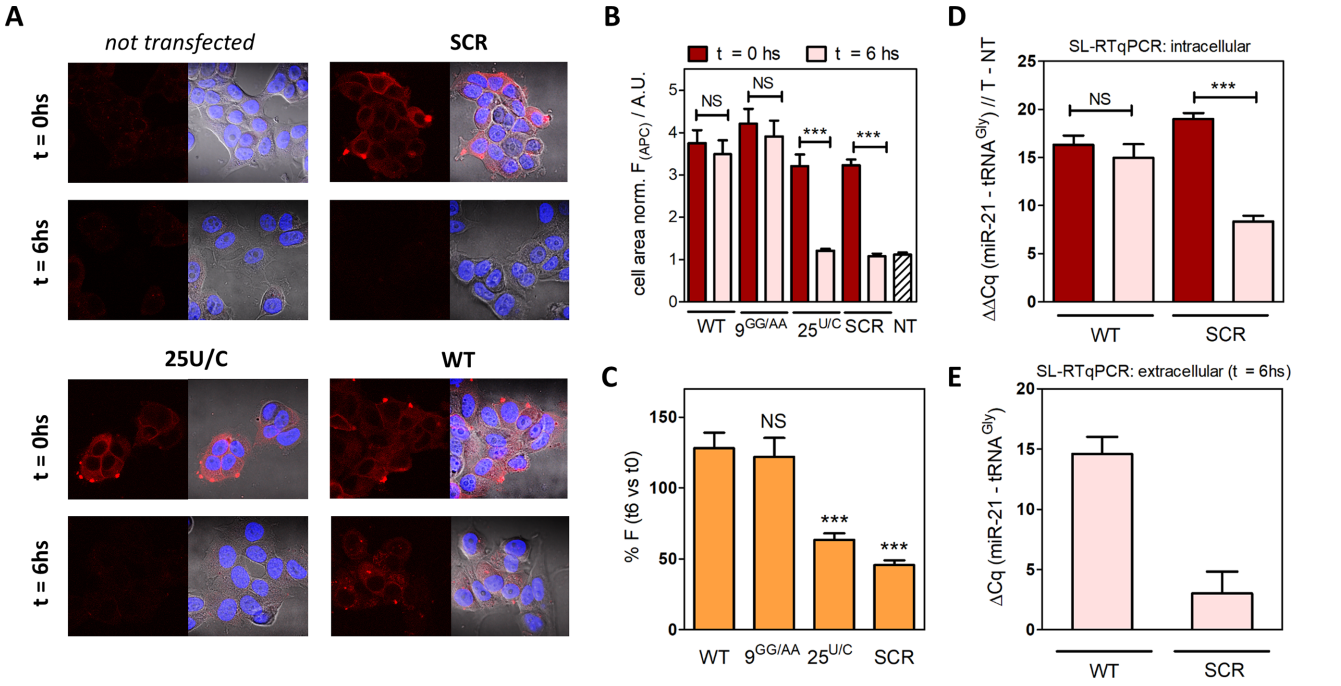

Figure 6. The dimerization capacity of $tRNA^{Gly}_{GCC}$ 5′ halves correlates with their intracellular stability. Biotinylated RNA oligonucleotides (100 nM) with the sequence of $tRNA^{Gly}$ 5′ halves (WT), the 9GG/AA and 25U/C mutants, or a scrambled version of WT where different bases were shuffled in order to disrupt folding and dimer interactions (SCR) were transfected in MCF-7 cells with cationic lipids. After incubation for 30 min at 37°C, cells were washed, and immediately fixed ($t0$) or incubated for further 6 h (t6) before fixing. Cells were then incubated with streptavidin conjugated to APC, and subjected to fluorescence microscopy (**A**). A minimum of 45 random fields was analyzed and the total APC fluoresce was normalized to the cell area covered in each field (**B**). This experiment was repeated three times, in order to obtain the percentage of APC fluorescence per cell area between $t = 6$ hs and $t = 0$ (**C**). Intracellular levels of the transfected RNAs were also analyzed by SL-RT-qPCR, using miR-21-5p as a reference, and subtracting the ΔCq values between transfected and non-transfected cells (**D**). Measurements of transfected RNAs in the extracellular space after successive washing of the cells were also perform in order to address whether the decreased levels of SCR were due to degradation or preferential secretion (**E**). In all cases, statistical analysis corresponds to one-way ANOVA with Tukey post-hoc test. Significance was studied between specified conditions (A, B) or versus WT (C). ***$P < 0.0001$. NS: not significant ($P > 0.05$). NT: non-transfected cells.

tRNA population. Interestingly, analysis of collected fractions by SL-RT-qPCR showed that $tRNA^{Gly}_{GCC}$ 5′ halves peaked closer to the predicted dimer elution volume than to the tRNA peak, Figure 7B), with negligible detection at the elution volume corresponding to the monomers (∼12 ml). As a control, miR-21-5p (which amplifies similarly to $tRNA^{Gly}_{GCC}$ 5′ halves in MCF-7 intracellular extracts) (8) was only detected as a monomer. To exclude the possibility that our SL-RT-qPCR system was cross-reacting with mature tRNAs, we repeated the assay without heat-denaturing the RNA before reverse transcription (Figure 7C and D), confirming an amplification maximum in the expected dimer fractions and inconsistent with the elution profile of full-length tRNAs. Furthermore, bands of ∼30 nt appeared when the same fractions were analyzed by gel electrophoresis under denaturing conditions (Figure 7E and F) including those where full-length tRNAs were virtually undetectable (Ve = 10.7 ml). Overall, these results strongly suggest that endogenous $tRNA^{Gly}_{GCC}$ 5′ halves are present in the intracellular compartment as dimers.

DISCUSSION

While certain specific small RNA families are present in some organisms and absent in others (indicative of their first appearance in evolution and later lineage-specific losses) (26), tRNA-derived fragments have been reported in virtually any organism in which they were looked for. Abundant cellular non-coding RNAs can be cleaved to produce fragments in a regulated fashion (9,10,27) or constitute relatively stable degradation intermediates easily detectable by high throughput sequencing or Northern blot. In any case, evidence is accumulating that at least some of these fragments can play various roles inside or between cells that are not necessarily related to the molecular function of their precursors (18).

tRNA-derived fragments (including the shorter tRFs and the larger tRNA halves) have long been recognized as a new family of small regulatory RNAs present in all kingdoms of life (28–33). In mammals, some of their documented roles are related to translation inhibition and stress-response (11,13) and the silencing of transposable elements, which has been shown both for short 18–22 nt tRFs (34) and longer 30–31 nt tRNA halves (19).

The involvement of tRNA-derived fragments in gene silencing is sequence-based. We speculated that structural constraints might also be functionally relevant. Structure may specify interactions in an aptamer-like fashion or increase the half-life of the RNAs by rendering them less prone to degradation. In support of the former, it has been shown that the oligo-guanine motif present in the extreme of $tRNA^{Ala}$ and $tRNA^{Cys}$ 5′ halves is necessary for their in-

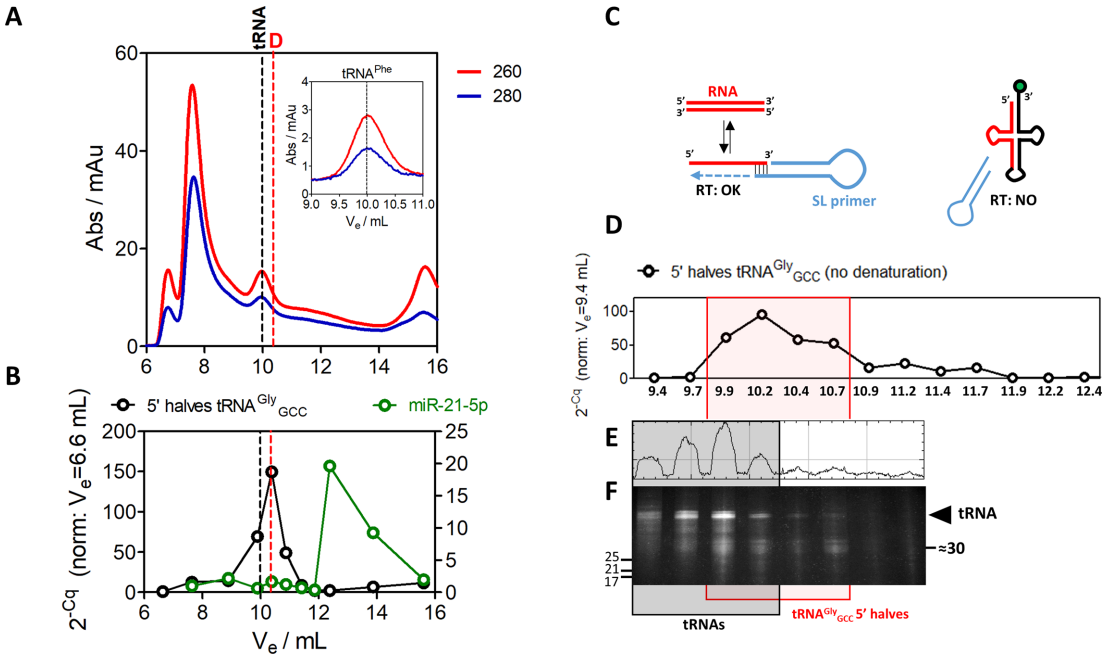

Figure 7. Endogenous $tRNA^{Gly}_{GCC}$ 5′ halves elute as dimers in MCF-7 cell lysates. MCF-7 cells were lysed in PBS + 0.1% sodium dodecyl sulfate. Filtered and centrifuged lysates were injected in a Superdex S75 10/300 column (**A**). In parallel, a gel-purified commercial yeast $tRNA^{Phe}$ standard was run, confirming the OD260 peak at Ve = 10.0 ml corresponds to full-length mature tRNAs (inset). Analysis of $tRNA^{Gly}_{GCC}$ 5′ halves by SL-RT-qPCR (**B**) showed maximum amplification in fractions closer to the dimer peak (Ve = 10.3 ml) than to the tRNA peak (black, left axis). As a control, miR-21-5p was only amplified in fractions corresponding to monomeric forms (green, right axis). Quantification cycles (Cq) were converted to linear scale (expressed as 2^{-Cq}), and normalized to the value at the exclusion volume (Ve = 6.6 ml). We repeated SL-RT-qPCR of collected fractions (in the 9.4–12.4 ml range, normalizing to Ve = 9.4 ml) but avoided heating the samples before reverse transcription (**C**). The amplification profile (**D**) was shifted two fractions (0.50 ml) to the right respect to the elution profile of full length mature tRNAs. This was assessed by running each fraction (after concentration by ethanol precipitation) in a 15% denaturing (7 M urea) polyacrylamide gel, and staining with SYBR gold (**E** and **F**). Densitometry analysis (E) was performed with the ImageJ software by plotting the gray value across a line spanning all lanes of the gel, at the migration line corresponding to full-length tRNAs.

teraction with the translation regulator YB-1 (11) and for their G quadruplex-mediated tetramerization (13,23). This strongly suggests that it is the structure that mediates the interaction with the protein, although the role of these tRNA halves in inhibiting translation initiation goes beyond their interaction with YB-1 (35). In support of the latter, we have demonstrated here that the capacity of $tRNA^{Gly}$ 5′ halves to form homodimers correlates with their intracellular and *in vitro* stability, and may explain the remarkable extracellular stability observed for these small RNAs.

The mechanism underlying the release of tRNA-derived fragments from cells leading to the non-EV extracellular fraction is still a matter of investigation. The 5′ tRNA halves studied herein can be secreted from cells as such or, alternatively, be a consequence of extracellular tRNA cleavage. This idea is particularly attractive because Angiogenin, the endonuclease responsible for the biogenesis of tRNA halves, is secreted (9,10). Furthermore, the recombinant RNAse inhibitor we used in Figure 1 actually corresponds to the natural Angiogenin inhibitor in the cytoplasm, though it has a broad spectrum for RNase A, B, and C family members in general. Specific sequencing techniques different from those used in this study are needed to retrieve full-length tRNAs (36–39), which can outnumber tRNA-derived fragments in the extracellular space (40). Nevertheless, we have shown that a variety of small RNAs (including rRNA and snoRNA-derived sequences) can be sequenced in the 'H' peak of cell-conditioned medium when inhibiting RNase activity, while $tRNA^{Gly}$ and $tRNA^{Glu}$ 5′ halves were essentially the only detectable species when the same techniques were applied in RNase-active medium. This strongly supports differential stability as a key aspect for the accumulation of specific tRNA halves in the extracellular space, though this does not exclude that differential secretion of tRNA halves or full-length tRNAs might contribute as well. In summary, four non-mutually exclusive scenarios can be envisioned to explain non-EV extracellular enrichment of $tRNA^{Gly}_{GCC}$ and $tRNA^{Glu}_{CUC}$ 5′ halves: (a) selective secretion of these fragments, (b) non-selective secretion of tRNA halves, and enrichment of these fragments because of their high extracellular stability, (c) selective secretion of full-length $tRNA^{Gly}$ and $tRNA^{Glu}$, and extracellular processing (e.g. by extracellular Angiogenin), (d) non-selective secretion of tRNAs, extracellular processing, and enrichment of the 5′ halves under study because of their differential extracellular stability.

Although we focused in $tRNA^{Gly}$ and $tRNA^{Glu}$ 5′ halves because of their abundance in the extracellular space of human cancer cell lines (8), their ability to form homo- or heterodimers might be also important for defining their intracellular concentration and function. Surprisingly, SL-RT-qPCR analysis of $tRNA^{Gly}_{GCC}$ 5′ halves in MCF-7 cell lysates showed maximum amplification in the fractions corresponding to the expected elution volume of the dimers, not the monomers. Furthermore, fractions which corre-

sponded to dimers or full-length tRNAs under native separation (i.e. SEC) revealed substantial amounts of RNAs ~ 30 nt under denaturing conditions (Figure 7). Although this could be explained by either nicked tRNAs or dimers of 5′ halves, the shift towards slightly higher elution volumes (i.e. more compact) of the fragments, and the amplification of tRNA halves by SL-RT-qPCR in the absence of heat denaturation strongly suggest the latter. Moreover, the dissociation constant for endogenous dimers seems to be much lower than measured for synthetic oligonucleotides, as the monomer/dimer ratio was greatly reduced in this experiment.

It will be worth studying whether single-point substitutions in $tRNA^{Gly}$ 5′ halves that are not capable of forming dimeric hybrids still retain the capacity to silence genes controlled by the endogenous retroelement MERVL in mouse embryos (19). Recent reports have also connected tRNA-derived fragments with LTR-retrotransposon control (34). Since these transposable elements use a tRNA molecule to prime reverse transcription, the idea that dimers of tRNA-halves could interfere (for example by competition) with these mechanisms is very attractive. Alternatively, dimerization can be dispensable for target recognition, but necessary to protect the RNAs from degradation, thereby increasing their extracellular half-life and/or intracellular steady-state levels. Since monomers and dimers are in dynamic equilibrium, the dimer might serve as a reservoir of functional monomer, or might be the functional entity by itself.

CONCLUSION

Our results demonstrate that it is the capacity of $tRNA^{Gly}$ 5′ halves to form homodimers, rather than their specific primary sequence, that dictates their intracellular stability. Although others have shown that aggregation of certain tRNA halves into tetrameric structures resistant to thermal and denaturing agent-mediated unfolding is functionally important (23), we provide the first evidence that intermolecular association of small RNAs can strongly impact their steady-state levels inside (and possibly also outside) live cells.

Is the tendency of tRNA-derived fragments to aggregate into supramolecular dsRNA-containing structures evolutionary ancient? It is well known that several tRNA genes in mammals contain introns with the two exonic sequences actually corresponding to 5′ and 3′ halves. Moreover, it has been shown that several Archaea combine separate genes coding for 5′ and 3′ halves (or even smaller fragments) in order to create functional tRNAs by trans-splicing (41–43). Some authors have proposed that modern cloverleaf tRNAs may have evolved by asymmetric association of genes coding for their 5′ and 3′ halves (18,44,45). Such a process would lead to high tRNA diversity from a smaller initial gene set. If this were the case, we speculate that afterwards, with 5′-3′ fusions present at the genomic level, tRNA fragmentation would be necessary to reconstitute 5′-5′ hybrids.

Besides evolutionary considerations, it is noteworthy that different human tRNA genes can produce 5′ halves with the capacity of forming homodimers or homotetramers. Although we have not provided a specific function for the dimers of $tRNA^{Gly}$ 5′ halves, we have shown dimerization renders the tRNAs less prone to degradation and increases the half-life of transfected synthetic RNAs in comparison with single-point mutants or shuffled sequences incapable of self-association. Overall, we would like to highlight that tRNA-derived fragments (and ncRNA fragments in general) are able to adopt specific secondary, tertiary and quaternary (i.e., intermolecular) structures that might also dictate function. Besides RNA/target RNA base-pairing interactions, our biochemical results point to a new layer of complexity at the three-dimensional level.

DATA AVAILABILITY

Sequencing data is available from the NCBI's small read archive (SRA) under the BioProject ID: PRJNA454316

SUPPLEMENTARY DATA

Supplementary Data are available at NAR Online.

ACKNOWLEDGEMENTS

The authors want to thank Ricardo Ehrlich, Mónica Marín and Tamara Fernández for fruitful discussions and for supplying yeast $tRNA^{Phe}$. Agustín Correa, Federico Carrión, Gonzalo Greif and Carlos Robello assisted with SEC, DSC and sequencing, respectively. The authors want to thank members of the following facilities at IPMon: UPR, UBP and UBM. Members of the Enzymology Lab (Faculty of Science, Universidad de la República) assisted with UV-melting experiments.

FUNDING

Comisión Sectorial de Investigación Científica (Universidad de la República, Uruguay); Agencia Nacional de Investigación e Innovación (ANII, Uruguay); FOCEM (MERCOSUR Structural Convergence Fund) [COF 03/11]. E.W. acknowledges the support of the LABEX 'ANR-10-LABX-0036_NETRNA'; French Embassy in Uruguay for travel expenses. J.P.T., S.P., L.D. and A.C. are researchers and received funding from PEDECIBA (Uruguay) and/or the Sistema Nacional de Investigadores (ANII, Uruguay). L.D. acknowledges ANII and IPMon for funding his postdoctoral fellowship. Funding for open access charge: IPMon intramural funds.
Conflict of interest statement. None declared.

REFERENCES

1. Valadi,H., Ekström,K., Bossios,A., Sjöstrand,M., Lee,J.J. and Lötvall,J.O. (2007) Exosome-mediated transfer of mRNAs and microRNAs is a novel mechanism of genetic exchange between cells. *Nat. Cell Biol.*, **9**, 654–659.
2. Witwer,K.W. (2015) Circulating microRNA biomarker studies: pitfalls and potential solutions. *Clin. Chem.*, **61**, 56–63.
3. Thomou,T., Mori,M.A., Dreyfuss,J.M., Konishi,M., Sakaguchi,M., Wolfrum,C., Rao,T.N., Winnay,J.N., Garcia-Martin,R., Grinspoon,S.K. *et al.* (2017) Adipose-derived circulating miRNAs regulate gene expression in other tissues. *Nature*, **542**, 450–455.
4. Sorrentino,S. (2010) The eight human "canonical" ribonucleases: molecular diversity, catalytic properties, and special biological actions of the enzyme proteins. *FEBS Lett.*, **584**, 2194–2200.

5. Vickers,K.C., Palmisano,B.T., Shoucri,B.M., Shamburek,R.D. and Remaley,A.T. (2011) MicroRNAs are transported in plasma and delivered to recipient cells by high-density lipoproteins. *Nat. Cell Biol.*, **13**, 423–433.
6. Wang,K., Zhang,S., Weber,J., Baxter,D. and Galas,D.J. (2010) Export of microRNAs and microRNA-protective protein by mammalian cells. *Nucleic Acids Res.*, **38**, 7248–7259.
7. Arroyo,J.D., Chevillet,J.R., Kroh,E.M., Ruf,I.K., Pritchard,C.C., Gibson,D.F., Mitchell,P.S., Bennett,C.F., Pogosova-Agadjanyan,E.L., Stirewalt,D.L. *et al.* (2011) Argonaute2 complexes carry a population of circulating microRNAs independent of vesicles in human plasma. *Proc. Natl. Acad. Sci. U.S.A.*, **108**, 5003–5008.
8. Tosar,J.P., Gámbaro,F., Sanguinetti,J., Bonilla,B., Witwer,K.W. and Cayota,A. (2015) Assessment of small RNA sorting into different extracellular fractions revealed by high-throughput sequencing of breast cell lines. *Nucleic Acids Res.*, **43**, 5601–5616.
9. Fu,H., Feng,J., Liu,Q., Sun,F., Tie,Y., Zhu,J., Xing,R., Sun,Z. and Zheng,X. (2009) Stress induces tRNA cleavage by angiogenin in mammalian cells. *FEBS Lett.*, **583**, 437–442.
10. Yamasaki,S., Ivanov,P., Hu,G.F. and Anderson,P. (2009) Angiogenin cleaves tRNA and promotes stress-induced translational repression. *J. Cell Biol.*, **185**, 35–42.
11. Ivanov,P., Emara,M.M., Villen,J., Gygi,S.P. and Anderson,P. (2011) Angiogenin-induced tRNA fragments inhibit translation initiation. *Mol. Cell*, **43**, 613–623.
12. Saikia,M., Jobava,R., Parisien,M., Putnam,A., Krokowski,D., Gao,X.H., Guan,B.J., Yuan,Y., Jankowsky,E., Feng,Z. *et al.* (2014) Angiogenin-cleaved tRNA halves interact with cytochrome c, protecting cells from apoptosis during osmotic stress. *Mol. Cell. Biol.*, **34**, 2450–2463
13. Ivanov,P., O'Day,E., Emara,M.M., Wagner,G., Lieberman,J. and Anderson,P. (2014) G-quadruplex structures contribute to the neuroprotective effects of angiogenin-induced tRNA fragments. *Proc. Natl. Acad. Sci. U.S.A.*, **111**, 18201–18206.
14. Honda,S., Loher,P., Shigematsu,M., Palazzo,J.P., Suzuki,R., Imoto,I., Rigoutsos,I. and Kirino,Y. (2015) Sex hormone-dependent tRNA halves enhance cell proliferation in breast and prostate cancers. *Proc. Natl. Acad. Sci. U.S.A.*, **112**, E3816–E3825.
15. Goodarzi,H., Liu,X., Nguyen,H.C., Zhang,S., Fish,L. and Tavazoie,S.F. (2015) Endogenous tRNA-Derived fragments suppress breast cancer progression via YBX1 displacement. *Cell*, **161**, 790–802.
16. Kim,H.K., Fuchs,G., Wang,S., Wei,W., Zhang,Y., Park,H., Roy-Chaudhuri,B., Li,P., Xu,J., Chu,K. *et al.* (2017) A transfer-RNA-derived small RNA regulates ribosome biogenesis. *Nature*, **552**, 57–62.
17. Rudinger-Thirion,J., Lescure,A., Paulus,C. and Frugier,M. (2011) Misfolded human tRNA isodecoder binds and neutralizes a 3′ UTR-embedded Alu element. *Proc. Natl. Acad. Sci. U.S.A.*, **108**, E794–E802.
18. Schimmel,P. (2017) The emerging complexity of the tRNA world: mammalian tRNAs beyond protein synthesis. *Nat. Rev. Mol. Cell Biol.*, **19**, 45–58.
19. Sharma,U., Conine,C.C., Shea,J.M., Boskovic,A., Derr,A.G., Bing,X.Y., Belleannee,C., Kucukural,A., Serra,R.W., Sun,F. *et al.* (2016) Biogenesis and function of tRNA fragments during sperm maturation and fertilization in mammals. *Science*, **351**, 391–396.
20. Dhahbi,J.M., Spindler,S.R., Atamna,H., Yamakawa,A., Boffelli,D., Mote,P. and Martin,D.I. (2013) 5′ tRNA halves are present as abundant complexes in serum, concentrated in blood cells, and modulated by aging and calorie restriction. *BMC Genomics*, **14**, 298.
21. Turchinovich,A., Weiz,L., Langheinz,A. and Burwinkel,B. (2011) Characterization of extracellular circulating microRNA. *Nucleic Acids Res.*, **39**, 7223–7233.
22. Akiyama,B.M., Laurence,H.M., Massey,A.R., Costantino,D.A., Xie,X., Yang,Y., Shi,P.Y., Nix,J.C., Beckham,J.D. and Kieft,J.S. (2016) Zika virus produces noncoding RNAs using a multi-pseudoknot structure that confounds a cellular exonuclease. *Science*, **354**, 1148–1152.
23. Lyons,S.M., Gudanis,D., Coyne,S.M., Gdaniec,Z. and Ivanov,P. (2017) Identification of functional tetramolecular RNA G-quadruplexes derived from transfer RNAs. *Nat. Commun.*, **8**, 1127.
24. Zuker,M. (2003) Mfold web server for nucleic acid folding and hybridization prediction. *Nucleic Acids Res.*, **31**, 3406–3415.
25. Boniecki,M.J., Lach,G., Dawson,W.K., Tomala,K., Lukasz,P., Soltysinski,T., Rother,K.M. and Bujnicki,J.M. (2016) SimRNA: a coarse-grained method for RNA folding simulations and 3D structure prediction. *Nucleic Acids Res.*, **44**, e63.
26. Fromm,B., Billipp,T., Peck,L.E., Johansen,M., Tarver,J.E., King,B.L., Newcomb,J.M., Sempere,L.F., Flatmark,K., Hovig,E. *et al.* (2015) A uniform system for the annotation of vertebrate microRNA genes and the evolution of the human microRNAome. *Annu. Rev. Genet.*, **49**, 213–242.
27. Emara,M.M., Ivanov,P., Hickman,T., Dawra,N., Tisdale,S., Kedersha,N., Hu,G.F. and Anderson,P. (2010) Angiogenin-induced tRNA-derived stress-induced RNAs promote stress-induced stress granule assembly. *J. Biol. Chem.*, **285**, 10959–10968
28. Martinez,G., Choudury,S.G. and Slotkin,R.K. (2017) tRNA-derived small RNAs target transposable element transcripts. *Nucleic Acids Res.*, **45**, 5142–5152.
29. Kumar,P., Mudunuri,S.B., Anaya,J. and Dutta,A. (2015) tRFdb: a database for transfer RNA fragments. *Nucleic Acids Res.*, **43**, D141–D145.
30. Gebetsberger,J., Zywicki,M., Künzi,A. and Polacek,N. (2012) tRNA-derived fragments target the ribosome and function as regulatory non-coding RNA in Haloferax volcanii. *Archaea*, **2012**, 260909.
31. Garcia-Silva,M.R., Frugier,M., Tosar,J.P., Correa-Dominguez,A., Ronalte-Alves,L., Parodi-Talice,A., Rovira,C., Robello,C., Goldenberg,S. and Cayota,A. (2010) A population of tRNA-derived small RNAs is actively produced in Trypanosoma cruzi and recruited to specific cytoplasmic granules. *Mol. Biochem. Parasitol.*, **171**, 64–73.
32. Lee,Y.S., Shibata,Y., Malhotra,A. and Dutta,A. (2009) A novel class of small RNAs: tRNA-derived RNA fragments (tRFs). *Genes Dev.*, **23**, 2639–2649.
33. Thompson,D.M., Lu,C., Green,P.J. and Parker,R. (2008) tRNA cleavage is a conserved response to oxidative stress in eukaryotes. *RNA*, **14**, 2095–2103.
34. Schorn,A.J., Gutbrod,M.J., LeBlanc,C. and Martienssen,R. (2017) LTR-Retrotransposon Control by tRNA-Derived Small RNAs. *Cell*, **170**, 61–71
35. Lyons,S.M., Achorn,C., Kedersha,N.L., Anderson,P.J. and Ivanov,P. (2016) YB-1 regulates tiRNA-induced Stress Granule formation but not translational repression. *Nucleic Acids Res.*, **44**, 6949–6960.
36. Gogakos,T., Brown,M., Garzia,A., Meyer,C., Hafner,M. and Tuschl,T. (2017) Characterizing expression and processing of precursor and mature human tRNAs by Hydro-tRNAseq and PAR-CLIP. *Cell Rep.*, **20**, 1463–1475.
37. Shigematsu,M., Honda,S., Loher,P., Telonis,A.G., Rigoutsos,I. and Kirino,Y. (2017) YAMAT-seq: an efficient method for high-throughput sequencing of mature transfer RNAs. *Nucleic Acids Res.*, **45**, e70.
38. Zheng,G., Qin,Y., Clark,W.C., Dai,Q., Yi,C., He,C., Lambowitz,A.M. and Pan,T. (2015) Efficient and quantitative high-throughput tRNA sequencing. *Nat. Methods*, **12**, 835–837.
39. Cozen,A.E., Quartley,E., Holmes,A.D., Hrabeta-Robinson,E., Phizicky,E.M. and Lowe,T.M. (2015) ARM-seq: AlkB-facilitated RNA methylation sequencing reveals a complex landscape of modified tRNA fragments. *Nat. Methods*, **12**, 879–884.
40. Shurtleff,M.J., Yao,J., Qin,Y., Nottingham,R.M., Temoche-Diaz,M.M., Schekman,R. and Lambowitz,A.M. (2017) Broad role for YBX1 in defining the small noncoding RNA composition of exosomes. *Proc. Natl. Acad. Sci. U.S.A.*, **114**, E8987–E8995.
41. Chan,P.P., Cozen,A.E. and Lowe,T.M. (2011) Discovery of permuted and recently split transfer RNAs in Archaea. *Genome Biol.*, **12**, R38.
42. Fujishima,K., Sugahara,J., Kikuta,K., Hirano,R., Sato,A., Tomita,M. and Kanai,A. (2009) Tri-split tRNA is a transfer RNA made from 3 transcripts that provides insight into the evolution of fragmented tRNAs in archaea. *Proc. Natl. Acad. Sci. U.S.A.*, **106**, 2683–2687.
43. Randau,L., Münch,R., Hohn,M.J., Jahn,D. and Söll,D. (2005) Nanoarchaeum equitans creates functional tRNAs from separate genes for their 5′- and 3′-halves. *Nature*, **433**, 537–541.
44. Kanai,A. (2015) Disrupted tRNA genes and tRNA fragments: a perspective on tRNA gene evolution. *Life (Basel)*, **5**, 321–331.
45. D.i Giulio,M. (2012) The origin of the tRNA molecule: independent data favor a specific model of its evolution. *Biochimie*, **94**, 1464–1466.